


# Critical Shifts in Cerebral White Matter Lipid Profiles After Ischemic–Reperfusion Brain Injury in Fetal Sheep as Demonstrated by the Positive Ion Mode MALDI-Mass Spectrometry

Cell Medicine  
Volume 12: 1–12  
© The Author(s) 2020  
Article reuse guidelines:  
sagepub.com/journals-permissions  
DOI: 10.1177/2155179019897002  
journals.sagepub.com/home/cmm  


Suzanne M. de la Monte<sup>1,2,3,4,5</sup> , Gina M. Gallucci<sup>4</sup>, Amy Lin<sup>4</sup>, Ming Tong<sup>4,5</sup>, Xiaodi Chen<sup>5,6</sup>, and Barbara S. Stonestreet<sup>5,6</sup>

## Abstract

Ischemic–reperfusion (I/R) injury to cerebral white matter during the perinatal period leads to long-term cognitive and motor disabilities in children. Immature white matter oligodendrocytes are especially vulnerable to metabolic insults such as those caused by hypoxic, ischemic, and reperfusion injury. Consequences include an impaired capacity of oligodendrocytes to generate and maintain mature lipid-rich myelin needed for efficient neuronal conductivity. Further research is needed to increase an understanding of the early, possibly reversible myelin-associated pathologies that accompany I/R white matter injury. This experiment characterized I/R time-dependent alterations in cerebral white matter lipid profiles in an established fetal sheep model. Fetal sheep (127 days gestation) were subjected to 30 min of bilateral carotid artery occlusion followed by 4 h ( $n = 5$ ), 24 h ( $n = 7$ ), 48 h ( $n = 3$ ), or 72 h ( $n = 5$ ) of reperfusion, or sham treatment ( $n = 5$ ). Supraventricular cerebral white matter lipids were analyzed using the positive ionization mode matrix-assisted laser desorption/ionization mass spectrometry. Striking I/R-associated shifts in phospholipid (PL) and sphingolipid expression with a prominent upregulation of cardiolipin, phosphatidylcholine, phosphatidylinositol monomannoside, sphingomyelin, sulfatide, and ambiguous or unidentified lipids were observed to occur mainly at I/R-48 and normalized or suppressed responses at I/R-72. In fetal sheep, cerebral I/R caused major shifts in white matter myelin lipid composition favoring the upregulated expression of diverse PLs and sphingolipids which are needed to support neuronal membrane, synaptic, metabolic, and cell signaling functions.

## Keywords

ischemia, demyelination, fetal development, white matter, reperfusion

## Introduction

Hypoxic–ischemic injury to the cerebral hemispheres in the perinatal period is the leading cause of long-term neurocognitive and motor deficits in children<sup>1</sup>. Ischemic injury causes tissue necrosis as the resulting critical reductions in blood flow compromise oxygen and nutrient delivery, threatening cellular energy metabolism and viability. Subsequent reperfusion could potentially salvage the injured tissue by flooding it with oxygenated blood and nutrients, but also could further damage the brain due to disruption of the blood–brain barrier and attendant calcium dyshomeostasis, oxidative stress<sup>2</sup>, and mitochondrial dysfunction. The resulting increase in mitochondrial permeability drives excess production of reactive oxygen species (ROS)<sup>3</sup>, damaging lipids and proteins, activating astrocyte and

<sup>1</sup>Department of Pathology and Laboratory Medicine, Providence VA Medical Center and the Women & Infants Hospital of Rhode Island, RI, USA

<sup>2</sup>Department of Neurology, Rhode Island Hospital, Providence, RI, USA

<sup>3</sup>Department of Neurosurgery, Rhode Island Hospital, Providence, RI, USA

<sup>4</sup>Department of Medicine, Rhode Island Hospital, Providence, RI, USA

<sup>5</sup>Alpert Medical School of Brown University, Providence, RI, USA

<sup>6</sup>Division of Neonatology, Department of Pediatrics, Women & Infants Hospital of Rhode Island, Providence, RI, USA

Submitted: May 5, 2019. Accepted: November 14, 2019.

### Corresponding Author:

Suzanne M. de la Monte, Rhode Island Hospital, 55 Claverick Street, Room 419, Providence, RI 02903, USA.

Email: Suzanne\_DeLaMonte\_MD@Brown.edu



microglial inflammatory responses<sup>4</sup>, and transducing proapoptosis cascades in neurons, glia, and vascular elements<sup>2</sup>. Repeated and sustained hypoxic–ischemic insults cause central white matter injury ranging from myelin loss to coagulative necrosis<sup>4</sup>. In premature neonates, white matter ischemic–reperfusion (I/R) injury can progress to periventricular leukomalacia<sup>1</sup>, particularly when the immature mediators of cerebral blood flow autoregulation sustain significant damage<sup>5</sup> and can no longer control reperfusion. A better understanding of the early stages of I/R injury linked to permanent structural and functional white matter pathologies could aid in the development of targeted neuroprotective approaches for preterm infants<sup>4</sup>.

The major components of white matter include (1) axons, which transmit signals across different brain regions; (2) oligodendrocytes, which produce and maintain myelin to facilitate neurotransmission; (3) astrocytes, which provide a supportive matrix; (4) microglia, which participate in immune surveillance and injury responses; and (5) blood vessels, which are needed to maintain cellular and tissue viability, supply nutrients, remove waste, and together with astrocytes, furnish the blood–brain barrier.

Oligodendrocytes are especially vulnerable to hypoxic, ischemic, and reperfusion injury. Dysfunction or loss of oligodendrocytes results in the degeneration of myelin in the central nervous system (CNS) and impairment of nerve impulse conductivity. Also, the loss of integrity of myelin renders exposed axons susceptible to ischemic, metabolic, and reperfusion injury. These complications are exacerbated in the developing brain because the immature oligodendrocytes exhibit particular sensitivity to I/R due to their high metabolic demands. Many critical functions of immature oligodendroglia, including the capacity to proliferate, migrate, and sustain myelin synthesis, maturation, and homeostasis, are compromised by oxidative stress, excitotoxicity, inflammation, and mitochondrial dysfunction. Although oligodendrocyte precursor cells (OPCs) proliferate in response to hypoxic–ischemic injury and could potentially replace lost oligodendrocytes, severe hypoxic–ischemic insults can compromise the maturation of OPCs, limiting their capacity to generate mature myelin to ensure axonal conductivity<sup>6</sup>. Therefore, therapeutic strategies to enhance survival and maturation of oligodendrocytes that have sustained significant hypoxic–ischemic–reperfusion injury could potentially facilitate axonal remyelination and restore neurotransmission<sup>7</sup> in order to prevent or reduce neurocognitive and motor deficits.

Myelin in the central nervous system has a high dry mass of lipids (70%–85%) compared to proteins (15%–30%). Major myelin lipids include cholesterol, glycosphingolipids, sulfatides (STs), gangliosides, phospholipids (PLs), and sphingomyelin (SM). Abnormal metabolism and expression of PLs and STs occur in many CNS diseases<sup>8–10</sup>. Membrane PLs regulate lipid rafts and receptor functions. Sulfatides, localized on the extracellular leaflets of myelin plasma membranes and synthesized by oligodendrocytes<sup>11</sup>, regulate neuronal plasticity,

memory, myelin maintenance, protein trafficking, adhesion, glial–axonal signaling, insulin secretion, and oligodendrocyte survival<sup>8</sup>. Sulfatide degradation via galactosylceramidase and sulfatidase yields ceramide<sup>11,12</sup>, which promotes neuroinflammation, increases ROS and apoptosis, and impairs cellular signaling through survival and metabolic pathways<sup>13</sup>. Reductions in ST content disrupt myelin's structure, function, and capacity to support neuronal conductivity<sup>13</sup>. Thus, imbalances in sphingolipid composition that reduce ST and increase ceramide probably act as important mediators of white matter (WM) degeneration.

Recent evidence indicates that alterations in white matter myelin lipid composition are found in many disease states including hypoxic–ischemic–reperfusion injury<sup>14</sup>. Despite considerable progress in understanding the effects of I/R on immature white matter oligodendroglia<sup>6</sup>, substantive information about the nature and degree of white matter lipid abnormalities or treatments that would be required to restore myelination in the developing brain is lacking. To address this question, we utilized matrix-assisted laser desorption/ionization (MALDI) mass spectrometry (MS) to characterize the alterations in cerebral white matter lipid expression that occurred within the very early time points following an I/R injury. The studies were performed in an established midgestation fetal sheep model<sup>15</sup> that mimics I/R injury in premature human infants.

For this study, the lipidomics data were acquired by the positive ion mode MALDI-MS. In a recent publication using the same model, we reported cerebral white matter lipidomics data acquired in the negative ion mode of MALDI-MS<sup>16</sup>. In contrast to the negative ion mode MALDI-MS which detects deprotonated lipid ions including phosphatidic acid (PA), phosphatidylethanolamine (PE), phosphatidylglycerol (PG), phosphatidylinositol, phosphatidylserine (PS), phosphatidylinositol phosphate, and ST<sup>17</sup>, the positive ion mode MALDI-MS favors the detection of protonated PLs, particularly phosphatidylcholine (PC), as well as ceramide, ganglioside, and SM<sup>17</sup>.

## Materials and Methods

### Experimental Model

We surgically prepared a fetal cerebral ischemia–reperfusion model at 118–122 days of gestation in mixed breed pregnant ewes<sup>15,18</sup>. Under 1% to 2% isoflurane anesthesia, the fetal carotid arteries were exposed, and then, the vertebral–occipital anastomosis and lingual arteries were ligated to restrict flow from the vertebral circulation and noncerebral vascular sources<sup>19</sup>. Two inflatable 4-mm vascular occluders were placed around each carotid artery to induce ischemia by inflating the occluders. Catheters were also placed in the brachial arteries and veins of the fetal sheep as previously described<sup>19</sup>. Reperfusion was achieved by deflating the occluders. Following recovery from surgery, on gestational days 125 to 130, 20

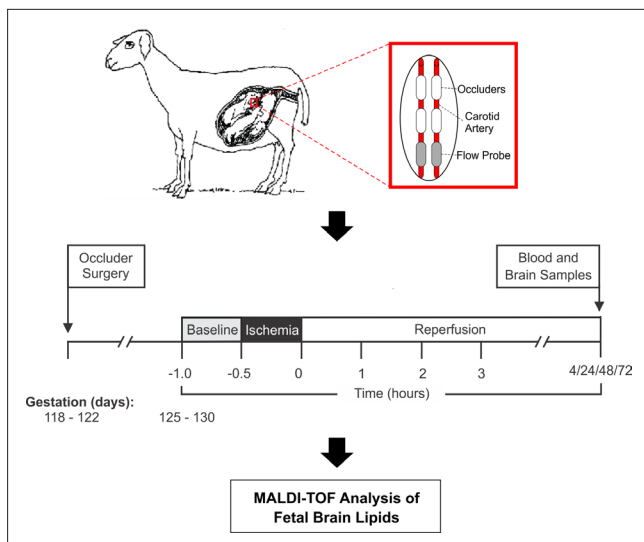


**Fig. 1.** Fetal sheep model of cerebral ischemic–reperfusion. Midgestation fetal sheep were subjected to 30 min of brain ischemia (green vertical bars) followed by 4 h ( $n = 5$ ), 24 h ( $n = 7$ ), 48 h ( $n = 3$ ), or 72 h ( $n = 5$ ) of reperfusion (red zones). Sham-instrumented controls (upper-most horizontal black line;  $n = 5$ ) were studied in parallel. Upon sacrifice, brains were harvested. Fresh frozen frontal supraventricular white matter was microdissected and the extracted lipids were used for matrix-assisted laser desorption/ionization time-of-flight analysis (see Materials and Methods).

ewes/fetal sheep were assigned to one of the five groups to examine the effects of 30-min ischemia followed by 4 h ( $n = 5$ ), 24 h ( $n = 7$ ), 48 h ( $n = 3$ ), or 72 h ( $n = 5$ ) of reperfusion<sup>15</sup> (Fig. 1). Control fetal sheep were instrumented but not exposed to cerebral ischemia ( $n = 5$ ). Just before sacrifice, mean arterial blood pressure, pH, arterial blood gases, glucose, and hematocrit values were obtained to assess the physiological status of the fetal sheep.

The ewes and fetuses were euthanized by intravenous pentobarbital (100–200 mg/kg). At the time of sacrifice, the fetal sheep were 80% to 85% of full gestation, and the brains of the fetal sheep at this time of gestation are approximately similar to near-term human infants<sup>19</sup>. Full-term gestation is 148 days. This research was approved by the Institutional Animal Care and Use Committees of the Alpert Medical School of Brown University and Women & Infants Hospital of Rhode Island, Providence, RI, USA (approval #1511000177). Postmortem fetal brains were removed promptly, and the samples of supraventricular and intragyral cerebral white matter were snap frozen in liquid nitrogen and stored at  $-80^{\circ}\text{C}$ .

### Lipid Extraction and MALDI

Standardized samples of fresh frozen fetal sheep white matter ( $50 \pm 5$  mg) were homogenized in 300  $\mu\text{L}$  of sterile deionized water with steel beads and a TissueLyser (Qiagen N.V., Venlo, Netherlands) was used for 3 min at 20 Hz. Lipids in 150  $\mu\text{L}$  of

each homogenate were extracted with 1 mL of  $\text{CHCl}_3:\text{MeOH}$  (2:1 v/v) according to the Folch method<sup>20</sup>. The dried pellets were solubilized in 200  $\mu\text{L}$  high performance liquid chromatography (HPLC)-grade methanol and mixed at a 1:1 ratio with 2,5-dihydroxybenzoic acid (Sigma-Aldrich, St. Louis, MO, USA) as matrix<sup>9</sup>. 2,5-Dihydroxybenzoic acid was prepared at a concentration of 75 mg/mL with HPLC-grade methanol as the solvent. Prepared sample aliquots (1  $\mu\text{L}$  each) were spotted in duplicate into a 384-well ground steel MALDI target plate (Bruker Daltonics, Bremen, Germany) along with mass calibration standards (Peptide Calibration Standard II, Bruker Daltonics, Bremen, Germany).

The samples were analyzed in the positive ion mode with the MALDI-tandem time-of-flight (TOF/TOF) Ultraflex extreme mass spectrometer (Bruker Daltonics, Billerica, MA, USA) as previously described<sup>9,21</sup>. In brief, data were acquired by delivering 3,200 shots at different locations within the spotted sample using the Smartbeam II Nd:YAG laser. External mass calibration was performed using a 1:1 mixture of standard peptides (Peptide Calibration Standard II, Bruker Daltonics, Bremen, Germany) and  $\alpha$ -cyano-4-hydroxycinnamic acid (Bruker Daltonics, Bremen, Germany).  $\alpha$ -Cyano-4-hydroxycinnamic acid (25 mg/mL) was prepared with TA-50 as the solvent. A total of 1  $\mu\text{L}$  of the standard was applied to the MALDI target plate. The mass calibration standards had masses ranging from 377 to 2,463 Da. Lipids with  $m/z$  values between 600 and 1,200 were analyzed in ClinProTools v3.0 (Bruker Daltonics, Bremen, Germany).

### Data Analysis

Matrix-assisted laser desorption/ionization data were processed using FlexAnalysis v3.4 (Bruker Daltonics, Billerica, MA, USA) and visualized with FlexImaging software v4.0 (Bruker Daltonics, Billerica, MA, USA). Results were analyzed using ClinProTools v3.0 (Bruker Daltonics, Billerica, MA, USA). Lipids were identified by their  $m/z$  values using the literature and LIPID MAPS (<http://www.lipidmaps.org/tools/index.html>) and confirmed by tandem mass spectrometry (MS/MS) in the LIFT-TOF/TOF mode<sup>22</sup>. Intergroup comparisons were displayed using data bar plots (Microsoft Excel 2016 Conditional Formatting; Microsoft Corporation, Redmond, WA, USA) and a heatmap. For the data bar plots, intergroup differences were analyzed using  $T$ -tests with a 5% false discovery rate (GraphPad Prism 7, La Jolla, CA, USA). For the heatmap, lipid profiles based on average intensities of expressed lipid ions and those associated with different durations of ischemia–reperfusion were compared in GeneCluster 3.0<sup>23</sup>. Hierarchical clustering was applied, and the dendrogram was displayed using Java TreeView<sup>23–25</sup>. Intergroup differences were compared by one-way analysis of variance (ANOVA) and the Tukey post hoc repeated measures test.  $\chi^2$  tests assessed proportional alterations in lipid subtypes after different durations of I/R (GraphPad Prism 7, La Jolla, CA, USA).

## Results

### Characteristics of the Experimental Model

The duration of pregnancy in sheep is 148 days, but fetal growth occurs mainly during the last 60 days of gestation. The I/R models were generated at the midpoint of the third trimester of pregnancy. There were no statistically significant intergroup differences in mean fetal gestational age, body weight, or brain weight (supplemental Table 1A), or the terminal mean levels of arterial PO<sub>2</sub>, PCO<sub>2</sub>, base excess, blood pressure, hematocrit, and glucose before sacrifice (supplemental Table 1B) by one-way ANOVA. Thus, the groups were well matched for subsequent comparisons.

### Lipid Ion Profiles

The Peak Statistic report identified 121 fetal sheep white matter lipids that had mass/charge (*m/z*) ratios between 706.6 and 1,596.0 Da. The lipids were identified using the LIPID MAPS database and the published literature, and by tandem mass spectrometry whenever the lipid identification required confirmation. The lipids detected are tabulated in ascending *m/z* order (supplemental Table 2B) and according to subtype (supplemental Table 2B). The lipid categories included (1) sphingolipids/glyceroceramides (*n* = 30; 24.8%), including 2 (1.6%) STs, 9 (7.4%) glycosphingolipids (ceramides and gangliosides), and 19 (15.7%) SMs; (2) PLs (*n* = 74; 61.2%), including 6 (4.9%) cardiolipins (CLs), 10 (8.3%) phosphatidylinositol mannosides (PIMs), 2 (1.6%) PAs, 38 (31.4%) PCs, 2 (1.6%) PEs, 2 (1.6%) PGs, and 14 (11.6%) PLs with head groups that could not be further identified (PL); (3) ambiguous (AMB) lipids (*n* = 7; 5.8%); or (4) unknown (UNK)/unidentified lipids (*n* = 10; 8.3%). C13-isotopes of PLs were grouped accordingly. Overall, PC comprised the largest single class of lipids detected, followed by SM (Fig. 2—normal fetal sheep white matter data). Cardiolipins, AMB lipids, other uncharacterized PLs, and UNK lipids comprised the middle group with each representing 5% to 12% of the lipids. Gangliosides, ceramides, ST, PA, PE, and PG each represented 1.6% to 4% of the lipids detected in the positive ionization mode. To avoid redundant representation of lipid data, C13 isotopes were excluded from the statistical analyses.

### Ischemic–Reperfusion Effects on White Matter Lipid Profiles Demonstrated by $\chi^2$ Tests and Principal Component Analysis

To determine if I/R significantly altered white matter lipid profiles,  $\chi^2$  tests were used to compare the percentages of samples within each group that had above-threshold levels of lipid ion expression (supplemental Fig. S1). Ninety-seven (79.5%) of 121 lipids detected in the positive ion mode were expressed in all samples, whereas 23 (18.9%) were expressed only transiently after I/R and 2 (1.6%) were detected de novo

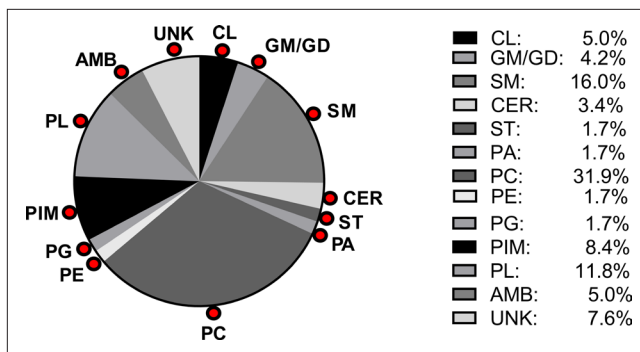


**Fig. 2.** Pie chart showing percentages of each lipid subtype detected in control fetal sheep cerebral white matter by matrix-assisted laser desorption/ionization time-of-flight in the positive ionization mode. The lipids were identified as PA = phosphatidic acid; PC = phosphatidylcholine; PE = phosphatidylethanolamine; PG = phosphatidylglycerol; PIM = phosphatidylinositol mannoside; PL = phospholipid not further characterized; CER = lactosylceramides; GM/GD = ganglioside; SM = sphingomyelin; ST = sulfatide; AMB = ambiguous; or UNK = unknown. The numerical percentages of each lipid depicted in the pie chart are shown in the legend.

at all I/R time points but not in controls.  $\chi^2$  tests revealed significant intergroup differences related to the proportions of samples that expressed PC(40:4) *m/z* 838.7, LPIM6 (16:0) *m/z* 1,545.2, a nonspecified PL (*m/z* 1,516.2), ST(36:2) *m/z* 844.6, and an AMB lipid (*m/z* 825.6); and trend effects for PC(P-38:6)/PC(36:0) *m/z* 790.6, PC(36:0) *m/z* 812.6, an indeterminate PL (*m/z* 827.6), and CL(78:0)/CL(78:8) *m/z* 1,572.2. These effects were mainly due to transient selective loss of a specific lipid that was abundantly expressed in the sham control or the 72-h I/R group, or transiently increased expression of a lipid ion following I/R that was not modulated in control samples.

Further comparisons of the I/R effects were made using principal component analysis (PCA) plots depicting the full spectra of white matter lipids expressed in each group. The PCA plots showed extensive overlap by two-way comparisons between control and each experimental group (Fig. 3), corresponding to the relatively few lipids that were expressed de novo or lost following I/R as illustrated in supplemental Fig. S1. These findings led to further studies to determine if I/R duration significantly altered the expression levels of specific lipids.

### Heatmap Analysis of Lipids Expressed in Relation to I/R Duration

The time-dependent effects of I/R on the relative levels of white matter lipids were depicted using a Java TreeView-generated heatmap with hierarchical clustering (Fig. 4). Lipids not detected in all the groups were excluded from the heatmap. Two broadly clustered effects of I/R were observed: The a1 cluster generally shows low levels of lipid expression in

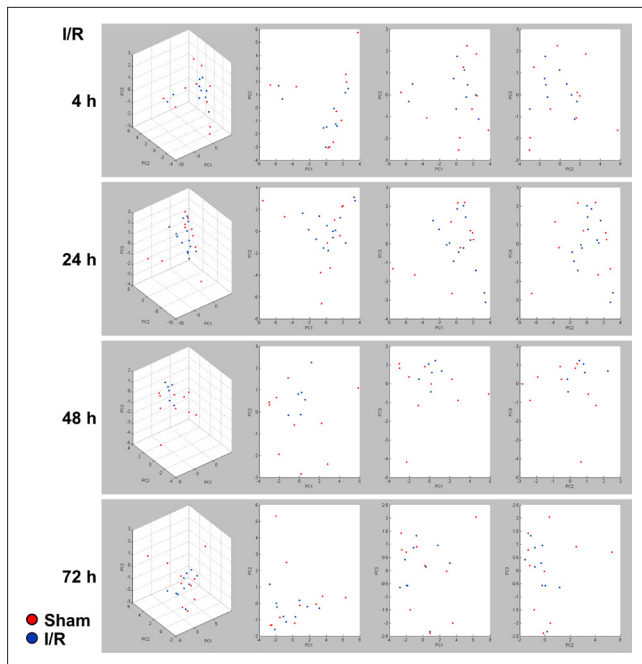


**Fig. 3.** Principal component analysis of white matter lipid profiles. Matrix-assisted laser desorption/ionization time-of-flight (positive ion mode) lipid data (600–1,000 Da mass range) were compared between sham controls (red) and fetal sheep subjected to I/R (blue) with 30 min of ischemia and 4, 24, 48, or 72 h of reperfusion. Principal component analysis plots were generated with ClinProTools. Note the considerable overlap of the control and ischemic–reperfusion clusters at all time points.

control white matter, while the a2 cluster depicts mainly high levels of lipid expression in control white matter. Intergroup differences were assessed by one-way ANOVA and the Tukey post hoc test. Significant differences are color coded in the figure.

The a1 cluster had 6 subclusters: b1, the largest cluster, was subdivided into b2 through b5. Cluster b2 was associated with similarly increased lipid expression at all time points relative to control, whereas b3 and b4 were associated with the low-level lipid expression at I/R-4, similar to control, progressive upregulated lipid expression at I/R-24 and I/R-48, with peak responses occurring after 48 h of reperfusion, followed by modest (b3) or sharply (b4) reduced lipid expression at the 72-h time point (Fig. 4). In addition, samples within the b4 cluster exhibited virtually normalized levels of lipid ion expression at I/R-72. In subcluster b5, white matter lipid expression was midrange in controls, sharply reduced at I/R-4, and then elevated to similar or higher control levels at I/R-24, I/R-48, and I/R-72. The pattern in Cluster b6 was similar to b5, except that basal expression in controls varied from low to midrange.

The a2 cluster, which was mainly associated with high levels of lipid expression in control brains, was subdivided into c1, c2, and c3 clusters. In c1, lipid expression was broadly

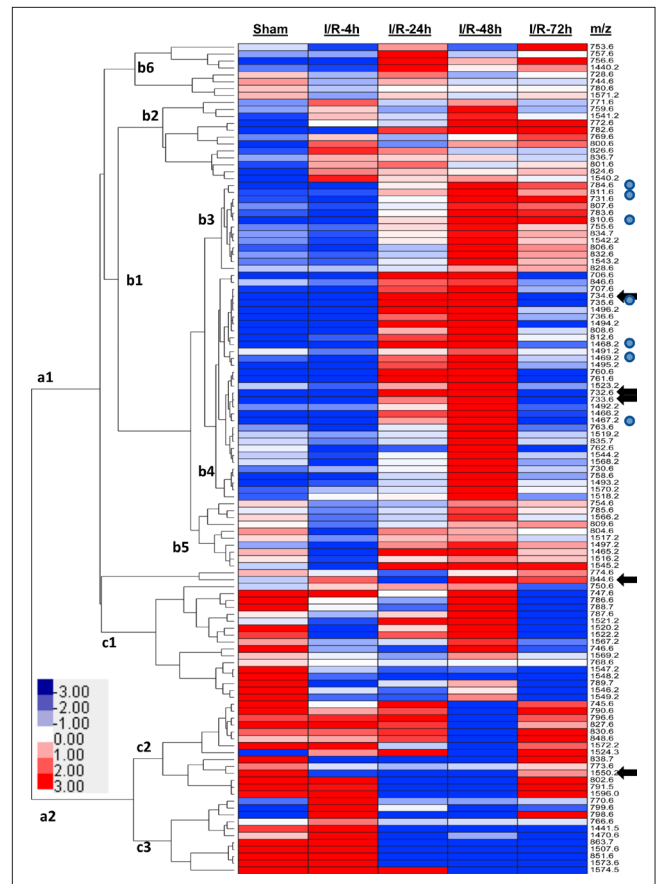


**Fig. 4.** Heatmap illustrating ischemic–reperfusion's duration effects on the relative expression levels of frontal white matter lipids. Fetal sheep were subjected to 30 min of ischemia followed by 4 h (I/R-4h), 24 h (I/R-24h), 48 h (I/R-48h), or 72 h (I/R-72 h) of reperfusion. Results were compared to the sham-operated controls. Ion intensities are displayed using a 7-color palette corresponding to z-scores scaled to have a mean of 0 and a standard deviation of 3.0. *m/z* values appear on the right-hand side. Hierarchical clustering dendrograms are shown. Two main clusters (a1 and a2) demonstrate broad and progressive effects of ischemic–reperfusion. Subclustered responses with a1 are represented by b1–b6, and for a2, by c1–c3. One-way ANOVA tests detected significant intergroup differences (black arrows:  $P < 0.05$  or better) or trend effects (blue dots:  $0.10 < P < 0.05$ ) of ischemic–reperfusion on the expression patterns and levels of 12 lipids. The main goal of this figure is to illustrate color-coded differences in white matter lipid expression based on hierarchical clustering which shows that the responses are patterned.

reduced at I/R-4 and I/R-24 and sharply increased toward control levels at I/R-48, while reducing to the lowest levels at I/R-72. For the c2 and c3 subclusters, high levels of lipid expression were present in control and I/R-4 groups, but lower in the I/R-24 and I/R-48 groups. In the c2 subcluster, lipid expression increased with the duration of I/R, eventually approaching control levels, whereas in the c3 subcluster, lipid expression remained suppressed across the time-span of I/R (Fig. 4). One-way ANOVA tests demonstrated significant intergroup

differences for 734.6, 732.6, 733.6, 844.6, and 1,550.2, and trend effects for 1,467.2, 1,469.2, 1,468.2, 735.6, 810.6, 811.6, and 784.6, indicating pronounced variability in lipid expression in relation to I/R duration (Fig. 4).

### Data Bar Displays of the Relative Effects of I/R on Lipid Ion Abundance

The ANOVA tests detected relatively few significant ( $n = 5$ ) or trend effects ( $n = 7$ ) due to progressive but overlapping reperfusion-duration responses that were often resolved or nearly normalized by I/R-72. Therefore, to further assess the specific effects of I/R duration on lipid expression relative to control, the mean peak intensities (reflecting lipid abundance) were compared by *T*-test analysis using a 5% false discovery rate to correct for multiple comparisons. The relative effects of I/R duration across the full spectrum of lipids were compared by calculating the percentage differences in mean expression relative to control, which were displayed using bar plots with results first subcategorized by lipid class and then sorted by *m/z* (Fig. 5). Bars to the left of the median axis reflect I/R-associated reductions in lipid expression and those to the right indicate I/R-mediated increases in lipid expression relative to control. Significant differences based on the mean levels of lipid expression are shown with color codes to the right of each bar plot.

### Overall Effects of I/R on Lipid Expression (Fig. 5)

Generalizable effects of I/R on white matter lipid expression were as follows: (1) the smallest differences from control typically occurred at I/R-4, whereas the largest differences mainly occurred at I/R-48; (2) the directional responses at I/R-4 were frequently opposite to those that were observed at I/R-24, I/R-48, and I/R-72; (3) with increasing duration of reperfusion, 57% of the lipids increased in expression, whereas 8% declined, and 35% were modulated by less than 5%, that is, their mean levels were virtually unchanged relative to control; and (4) the responses at I/R-72 were muted primarily in comparison with I/R-48, but in some instances, I/R-24 as well. *T*-tests demonstrated significant or trend effect differences in mean expression of 17 (14.0%) lipids at I/R-4, 23 lipids at I/R-24 (19.0%), 47 (38.8%) lipids at I/R-48, and 25 (20.7%) lipids at I/R-72.

### Effects of I/R on the Expression of Specific Lipid Subtypes

**CARDIOLIPIN.** Cardiolipins are mitochondria-specific PLs that maintain integrity and functionality of membranes<sup>26</sup>. Among 6 CLs that were detected in the white matter, CL (*m/z* 1,441.6) exhibited significantly increased expression at I/R-4 followed by reduced expression with longer periods of I/R, whereas CL (*m/z* 1,572.2) was consistently reduced throughout the I/R time course. However, 4 of 6 CLs exhibited

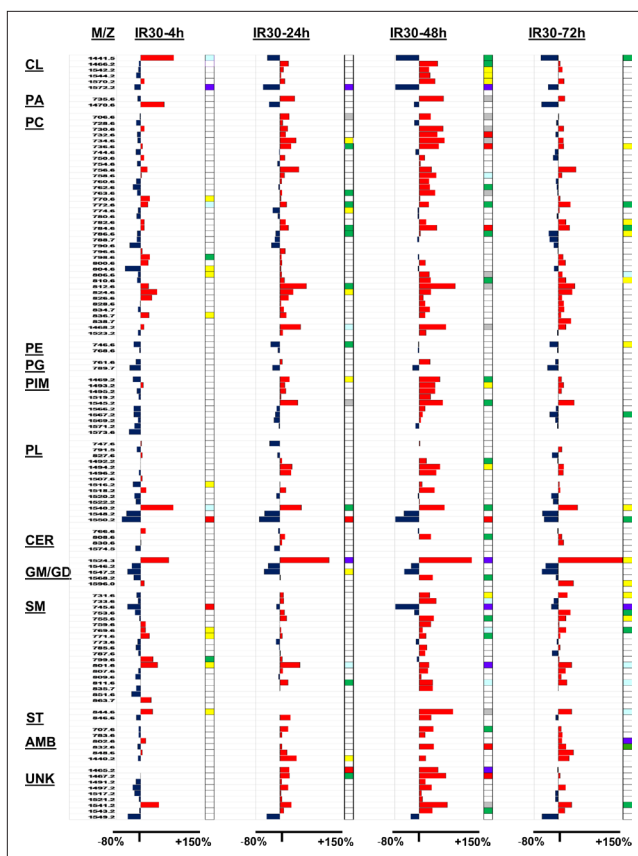


**Fig. 5.** Data bar plot illustrates paired analyses of ischemic-reperfusion's effects on relative mean lipid ion abundance after 30 min of ischemia followed by 4 h (IR30-4h), 24 h (IR30-24h), 48 h (IR30-48h), or 72 h (IR30-72h) of reperfusion. Blue bars to the left indicate I/R-associated reductions in lipid expression relative to control and red bars to the right reflect increases in lipid expression. The lipids were first grouped by their subtypes and then sorted by *m/z*. The lipid subtypes and *m/z* values are listed to the left. CL = cardiolipin; PA = phosphatidic acid; PC = phosphatidylcholine; PE = phosphatidylethanolamine; PG = phosphatidylglycerol; PIM = phosphatidylinositol mannoside; PL = phospholipid with unknown head group; Cer = galactosylceramide/glucosylceramide; GM/GD = ganglioside; SM = sphingomyelin; ST = sulfatide; AMB = ambiguous; UNK = unknown. Intergroup comparisons were made using *T*-tests with 5% false discovery rates (yellow =  $0.10 < P < 0.05$ ; green =  $P < 0.05$ ; pale blue =  $P < 0.01$ ; gray =  $P < 0.005$ ; red =  $P < 0.001$ ; and violet =  $P < 0.0001$ ). The very small font corresponding to the *m/z* values is used with the goal of showing responses of all lipids in a single figure, focusing on group trends rather than individual white matter lipid responses.

minimal shifts in expression at all time points except I/R-48 when significant or statistical trend peak increases were detected relative to control.

**PHOSPHATIDIC ACID.** Phosphatidic acids are structural components of cell membranes and have functional roles in intracellular signaling during growth and proliferation<sup>27</sup>. Two PAs detected had opposite time course responses with I/R.

Phosphatidic acid ( $m/z$  735.6) was initially unchanged at I/R-4, then progressively and ultimately significantly upregulated from I/R-24 to I/R-48, and finally, relatively normalized. Phosphatidic acid ( $m/z$  1,470.6) was initially elevated at I/R-4 (not significant), but subsequently minimally altered or modestly reduced relative to control.

**PHOSPHATIDYLCHOLINE.** Phosphatidylcholines comprise the majority of eukaryotic cell membrane lipids and have important roles in signal transduction. Disruption of PC homeostasis can lead to cellular apoptosis<sup>28</sup>. Ischemic–reperfusion increased the expression of 25 PCs (66%), modestly reduced the expression of 4 PCs (10%), and minimally altered the expression of 9 PCs (24%). Although modestly upregulated PC expression was detectable at I/R-4 in some instances, progressive and often statistically significant increases mainly occurred from I/R-24 to I/R-48. By I/R-72, the levels had declined from their peak responses but still moderately or significantly higher than control. Although several PCs were reduced at various I/R time points relative to control, for the most part, statistically significant or trend effects were not observed.

**PHOSPHATIDYLETHANOLAMINE.** Phosphatidylethanolamines are structural components of the inner leaflet of plasma membranes<sup>29</sup>. Only 2 PEs were detected in the positive ion mode of MALDI. Phosphatidylethanolamine ( $m/z$  746.6) was significantly or trend-wise inhibited relative to control at I/R-24 and I/R-72. In contrast, PE ( $m/z$  768.6) was unaffected by I/R.

**PHOSPHATIDYLGLYCEROL.** Phosphatidylglycerols have important roles in maintaining cell membrane homeostasis<sup>30</sup>. Only 2 PGs were detected. The effects of I/R varied but there were no significant or trend effects detected relative to control.

**PHOSPHATIDYLINOSITOL MONOMANNOSIDES.** This lipid subtype has no known function in mammalian cells<sup>31</sup>. Thus far, PIMs have been characterized only in relation to prokaryotic organisms in which they provide lipid anchors of lipoglycans, lipomannan, and lipoarabinomannan<sup>32</sup>. Nonetheless, PIMs and LPIMs were detected in brains of both control and I/R-treated fetal sheep. PIM/LPIM  $m/z$  1,469.2, 1,493.2, 1,495.2, 1,519.2, and 1,545.2 exhibited clustered progressive upregulated expression from I/R-24 to I/R-48, followed by modest declines at I/R-72. In contrast, PIM/LPIMs with  $m/z$  1,566.2 to 1,573.6 exhibited modest inhibitory or minimal responses to I/R.

**PHOSPHOLIPIDS.** A total of 14 PLs could not be further categorized. The PL responses to I/R varied over the time course, but 6 exhibited progressive patterned alterations in expression with the duration of reperfusion such that 4 lipids increased from I/R-4 to I/R-48 then declined somewhat by I/R-72 and 2 remained consistently reduced relative to

control over the full-time course of study. In contrast, I/R had minimal or no consistent effect on the expression of 8 PLs.

**CERAMIDE.** Galactosylceramide (GalCer) is the most abundant glycolipid in myelin<sup>33</sup>, and glucosylceramide (GlcCer) is a precursor for generating lactosylceramides<sup>34</sup>. Four Cer species were detected. Overall responses to I/R were minimal except for GlcCer (40:1;  $m/z$  808.6) which exhibited increased expression at I/R-24 and significantly elevated peak levels at I/R-48.

**GANGLIOSIDES.** Gangliosides are generally located on the outer surface of plasma membranes and regulate cell-to-cell interactions<sup>35</sup>. Ischemic–reperfusion had variable effects on the expression levels of 5 white matter gangliosides. Two were moderately reduced from I/R-4 to I/R-72. One was prominently increased at I/R-4, I/R-24, and I/R-72, but unchanged at I/R-48 relative to control. Two others had moderately reduced expression over the full I/R time course. Two were significantly or trend-wise increased at either I/R-48 or I/R-72, and the remaining one, GD1a ( $m/z$  1,524.3), exhibited striking and consistently greater levels expression relative to control from I/R-4 to I/R-72.

**SPHINGOMYELIN.** Sphingomyelins help to compartmentalize signaling events and promote neuronal differentiation, synapse formation, synaptic transmission, and glial–neuronal interactions in the CNS<sup>36</sup>. Among 19 SMs detected, I/R increased the expression of 14 (73.7%) at one or more time points, and for the most part, peak-level stimulation occurred at I/R-48 followed by I/R-72. Modest inhibitory responses occurred mainly at I/R-4.

**SULFATIDE.** Sulfatides assist in stabilizing plasma membranes<sup>37</sup>. Two STs were detected. Both were mainly increased by I/R and had peak responses at I/R-48.

**AMBIGUOUS LIPIDS.** A total of 6 lipids were designated as AMB because their  $m/z$ 's corresponded to 2 or more lipids in the LIPID MAPS database. At I/R-4, the levels of lipid expression were similar to control, but at I/R-24, I/R-48, and/or I/R-72, the expression was sharply increased relative to control for 5 of 6 (83%) AMB lipids.

**UNKNOWN/UNIDENTIFIED LIPIDS.** A total of 9 lipids were designated as UNK because they could not be identified from the LIPID MAPS database or published literature. As a group, most were either modestly inhibited or unchanged at I/R-4, but after longer periods of reperfusion, their expression levels increased and tended to peak at I/R-48. In contrast, the expression levels of 1 UNK lipid ( $m/z$  1,549.2) were reduced relative to control at all I/R time points studied.

## Discussion

The primary goal of this research was to characterize the early biochemical abnormalities associated with perinatal cerebral I/R injury because attendant white matter damage can lead to long-term cognitive and motor disabilities. Since immature oligodendrocytes are especially vulnerable to metabolic insults such as those caused by hypoxic, ischemic, and reperfusion injury, and their main functions include synthesis and maintenance of lipid-rich myelin which is needed for efficient neuronal conductivity, we hypothesized that the associated impairments in oligodendroglial function would be marked by substantial alterations in white matter myelin lipid composition. Improved understanding of oligodendroglial and myelin-associated responses to injury, particularly in the early stages, could lead to new strategies for reducing, reversing, or limiting their long-term adverse effects. Herein, we used MALDI-MS to assess shifts in myelin lipid profiles that occur after 30 min of ischemia followed by up to 72 h of reperfusion in an established midgestation fetal sheep model<sup>15,18,19</sup>.

Matrix-assisted laser desorption/ionization time-of-flight enables high throughput lipidomics analysis of white matter myelin abnormalities linked to various diseased states including injury and degeneration. The expanded use of this investigational tool could facilitate highly sensitive diagnostic applications. Despite the rapid growth in structural analysis, the regulation of biosynthesis, turnover, and function of specific lipid ions has not been well documented. Moreover, since specific classes of lipids may share similar functions, their expression levels may be coordinated<sup>16</sup>. One goal of lipidomics profile research is to identify clustered responses that characterize disease states.

White matter lipids in the CNS include cholesterol, glycosphingolipids, STs, gangliosides, and PLs consisting of glycerophospholipids (PA, PC, PE, PG, phosphatidylinositol (PI), PS, and plasmalogens), and SM. Sphingomyelin is composed of ceramide plus a phosphocholine or phosphoethanolamine polar head group. Several CNS diseases have already been linked to altered metabolism or expression of PLs and STs<sup>8</sup>, but the long-term functional consequences are poorly understood. This study employed the positive ionization mode MALDI-MS which is primarily suited for detecting protonated PLs, particularly PC, as well as SM, gangliosides, and ceramides.

The previous studies in the midgestation fetal sheep model demonstrated marked reductions in white matter myelin content within 48 h of I/R and little or no structural recovery over 72 h of reperfusion<sup>15</sup>. Instead, reactive inflammatory and astrocytic responses and oligodendrocyte loss accompanied the white matter damage, particularly at I/R-48 and I/R-72. Since the MALDI-MS studies were performed with lipids extracted from white matter, oligodendrocyte membranes and myelin were likely the main sources. Principal component analysis plots demonstrated that I/R

caused relatively few changes in the composition of lipids that were expressed. Instead, the major conclusion drawn from the heatmap and data bar plots was that cerebral I/R caused striking and rapid shifts in the expression levels of PLs and sphingolipids over the 72-h time course, with peak responses occurring mainly at I/R-48. Furthermore, for the most part, I/R increased the expression of CL, PC, phosphatidylinositol monomannoside, SM, and ST, which mainly contribute to the functional support of neuronal membranes, synapses, metabolism, and signal transduction.

The heatmap with hierarchical clustering demonstrated 2 broad patterns of dynamic shifting in the levels of lipids expressed over the time course of study. One broad group was characterized by abundant lipid expression in controls and reduced levels with I/R, while the other showed low levels of lipid expression in controls and striking upregulation in response to I/R, particularly at 24 h and later time points. The very early (4 h) generally inhibitory effects of I/R may have been due to acute oligodendrocyte injury and abrupt cessation of biosynthetic activity. In contrast, the subsequent striking and progressive increases or declines in lipid expression with increasing duration of reperfusion could have reflected (1) changes in oligodendrocyte metabolism leading to substantial alterations in cell membrane and myelin lipid composition; (2) increased inflammatory cell infiltration in response to injury; or (3) activation of astrocytes and vascular elements. The trends toward normalized lipid expression levels at I/R-72 are consistent with the concept that the earlier responses (I/R-24 and I/R-48) were likely reactive and transient, whereas the later responses beginning at I/R-72 were adaptive and possibly reflective of a return to metabolic homeostasis.

The data bar plots revealed that more than half of the CL, PC, PIM, SM, ST, AMB, and UNK/unidentified lipids and the GD1a [M1-Neu5Ac-CO2+Na]+ganglioside were increased by I/R, particularly at I/R-48. In contrast, the expression levels of 4 ceramides and 4 of 5 gangliosides were modestly altered and often inhibited by I/R. Conclusions cannot be drawn concerning PE, PG, or PA since only 2 of each were detected; one was increased and the other decreased by I/R. However, data captured by the negative ionization mode MALDI-MS more effectively revealed the time course effects of I/R on PA, PE, PI, and PG<sup>16</sup>, whereas the positive ionization mode MALDI-MS was more suitable for detecting PC and CL.

Since CL is uniquely localized in the inner mitochondrial membrane, comprises 20% of its lipid mass, and has a critical role in optimizing the function of mitochondrial enzymes<sup>38-41</sup>, its upregulated expression following I/R could represent a compensatory or reparative response needed to restore bioenergetics and sustain the viability of oligodendroglia. Furthermore, increased CL is neuroprotective via increased mitophagy which mediates the elimination of damaged mitochondria in the setting of traumatic brain injury induced ROS production and neuronal apoptosis<sup>42</sup>.



Phosphatidylcholines are major structural components of biological membranes and they are important sources of diacylglycerol and fatty acid-generated second messengers<sup>43</sup>. The previous reports showed that PC and PE expressions declined following global cerebral ischemia and do not subsequently increase with reperfusion<sup>44</sup>. Our discordant finding of increased PC expression after I/R may have been due to inherent differences between the present fetal model and the adult rat models utilized in the previous publications. In another study using adult rat brains, I/R increased PC[M+Na] and depleted PC[M+K] in injured brain regions<sup>45</sup>, whereas in fetal sheep white matter, we detected an elevated expression of [M+H]<sup>+</sup>, [M+Na]<sup>+</sup> and [M+K]<sup>+</sup>, particularly at I/R-24 and I/R-48. Conceivably, the I/R-associated striking increases in PC sodium, potassium, and hydrogen adduct ions observed in fetal sheep white matter may have been mediated by significant disruption of the blood–brain barrier and attendant massive cation influx with edema<sup>45</sup>.

Sphingolipids are derived from cell membranes and function as signaling molecules that mediate a broad range of functions including proliferation, survival, apoptosis, migration, and adhesion<sup>33,36,46</sup>. The upregulated expression of SM in fetal sheep white matter following I/R agrees with findings in the previous reports that showed sphingolipid accumulation during reperfusion and restoration of blood flow to ischemic brain tissue<sup>44,47</sup>. These responses may indicate that with increasing duration of reperfusion, compensatory processes become activated to help re-establish synaptic connectivity, glial–nerve interactions, neuronal repair and differentiation, and intracellular signaling<sup>36</sup>. On the other hand, studies in adult rat models showed that sphingolipid expression was significantly altered by cerebral ischemic injury and during postischemic repair<sup>48</sup> such that ischemic stroke led to progressive and sustained reductions in SM and increases in ceramide<sup>49</sup>. Mechanistically, SM hydrolysis via sphingomyelinase increased ceramide generation. Both the loss of SM and the accumulation of ceramide exacerbate brain injury. In our fetal sheep model, I/R prominently increased the expression of SMs. Those responses may have been protective or restorative as they were associated with either reduced or minimal change in the expression of all but one of the five ceramide species were detected.

Ceramides function as important second messengers in apoptosis and cellular signaling in response to stress, including ischemia/reperfusion<sup>50</sup>. Ceramides are generated via SM hydrolysis, recycling of complex sphingolipids, or de novo biosynthesis<sup>51</sup>. The previous studies reported that cerebral ceramide levels increase following I/R<sup>50</sup> or fetal asphyxia<sup>52,53</sup>. Ceramide accumulation due to SM hydrolysis is associated with declines in SM, which can occur with I/R injury<sup>50</sup>. In contrast after mild I/R, ceramide accumulates via de novo biosynthesis rather than SM degradation. Ischemic–reperfusion induced ceramide accumulation within mitochondria contributes to mitochondrial dysfunction<sup>54–56</sup>. In the present study, in light of the prominently increased expression of

SM, the selective increase in GlcCer (40:1) may have resulted from de novo synthesis in injured oligodendroglial cells. Alternatively, it could have been driven by the influx of inflammatory cells associated with responses to I/R injury<sup>57</sup>.

Gangliosides are synthesized from ceramide by sequential glycosyltransferase reactions used to add sugar moieties<sup>58</sup>. Since gangliosides have an important role in helping to maintain plasma membrane integrity, their transient upregulation with I/R may reflect a compensatory response to injury. However, of 5 gangliosides (sialylated glycosphingolipids) detected, only GD1a [M1-Neu5Ac-CO2+Na]<sup>+</sup> was strikingly elevated across most I/R time points. Although GD1a is normally expressed in gray matter, particularly the cerebral cortex, increased levels in the white matter have been observed in neurodegenerative diseases. The elevated levels of GD1a following I/R may have contributed to the white matter pathology by functioning as a nerve cell ligand for myelin-associated glycoprotein which inhibits nerve regeneration<sup>46</sup>, or as a driver of neuroinflammation via activation of brain microglia<sup>59</sup>.

Sulfatide is a major lipid component of CNS myelin and has broad functions related to developmental signaling, growth regulation, protein trafficking, neuronal plasticity, cell adhesion, and membrane structure<sup>60</sup>. However, in disease, ST may promote inflammation via aberrant activation of microglia and astrocytes and paradoxically may play a role in demyelination<sup>61</sup>. Therefore, the upregulated expression of ST following I/R could reflect a pro-inflammatory state corresponding with the progressive injury and degeneration of cerebral white matter observed in the fetal sheep model<sup>16</sup>.

## Conclusions

In conclusion, these studies identified major rapid reperfusion duration-dependent shifts in lipid composition within fetal sheep cerebral white matter following transient ischemia. Ischemic–reperfusion in fetal sheep causes pathophysiological changes reminiscent of those observed in white matter of preterm human infants<sup>6,62–64</sup>. The timing of injury in preterm infants cannot be ascertained easily in the clinical setting, and the overall impact of the injury cannot be determined until structural pathology, that is, cystic or diffuse white matter injury is detected by neuroimaging weeks or months after the initial insult<sup>65</sup>. The rapid shifts in lipid composition observed in fetal sheep brains indicate that I/R-related white matter injury in neonates begins long before it can be detected using the current ultrasound or magnetic resonance imaging, and highlights the need to develop more sensitive noninvasive biomarker assays.

The strength of this work was that a novel approach was applied to demonstrate early and progressive shifts in myelin lipid expression following I/R in an established fetal sheep model that shares properties with human preterm

infants. The use of MALDI-MS revealed significant alterations in myelin lipid composition corresponding to the effects of ischemia–reperfusion injury. The fact that significant differences were detected indicates that the study was adequately powered, despite relatively small group sizes. Nonetheless, future efforts should be directed toward repeating this study with larger sample sizes and longer durations of post-I/R recovery to assess long-term effects on WM myelin lipidomic development.

### Author Contributions

Suzanne M. de la Monte conceived of the collaborative research, directed and supervised the collection of primary data including sample analysis, analyzed the data, and wrote the manuscript. Gina M. Gallucci processed the brain samples for MALDI, performed bioinformatics analysis of the results, helped prepare the tables and graphs, and contributed to the preparation of the manuscript. Amy Lin performed bioinformatics analysis of the results, helped prepare the tables and graphs, and contributed to the preparation of the manuscript. Ming Tong organized and guided the brain sample processing for MALDI, and reviewed the manuscript. Xiaodi Chen generated the experimental model, provided critical results about the experimental model, and reviewed the manuscript. Barbara S. Stonestreet designed the in vivo experimental model and critically reviewed the manuscript.

### Ethical Approval

Ethical approval is not applicable for this article.

### Statement of Human and Animal Rights

All procedures in this study were approved and conducted in accordance with the Institutional Animal Care and Use Committees of the Alpert Medical School of Brown University and Women & Infants Hospital of Rhode Island, Providence, RI, USA (Approval #1511000177).

### Statement of Informed consent

There are no human subjects in this article and informed consent and human ethical approval is not applicable for this article.

### Declaration of Conflicting Interests

The author(s) declared no potential conflicts of interest with respect to the research, authorship, and/or publication of this article.

### Funding

The author(s) disclosed receipt of the following financial support for the research and/or authorship of this article: This research was supported by Grants AA11431, AA024092, NS096525, and HD057100 from the National Institutes of Health.

### ORCID iD

Suzanne M. de la Monte  <https://orcid.org/0000-0001-5886-2306>

### Supplemental Material

Supplemental material for this article is available online.

### References

1. Distefano G, Praticò AD. Actualities on molecular pathogenesis and repairing processes of cerebral damage in perinatal hypoxic-ischemic encephalopathy. *Ital J Pediatr.* 2010;36:63.
2. Torres-Cuevas I, Parra-Llorca A, Sánchez-Illana A, et al. Oxygen and oxidative stress in the perinatal period. *Redox Biol.* 2017;12:674-81.
3. Bakthavachalam P, Shanmugam PST. Mitochondrial dysfunction - Silent killer in cerebral ischemia. *J Neurol Sci.* 2017;375:417-423.
4. Hirayama J, Wagner SJ, Abe H, Ikebuchi K, Ikeda H. Involvement of reactive oxygen species in hemoglobin oxidation and virus inactivation by 1,9-dimethylmethylene blue phototreatment. *Biol Pharm Bull.* 2001;24:418-21.
5. Vesoulis ZA, Mathur AM, autoregulation C. Brain injury, and the transitioning premature infant. *Front Pediatr.* 2017;5:64.
6. Back SA. White matter injury in the preterm infant: pathology and mechanisms. *Acta Neuropathol.* 2017;134:331-49.
7. McIver SR, Muccigrosso M, Gonzales ER, et al. Oligodendrocyte degeneration and recovery after focal cerebral ischemia. *Neuroscience.* 2010;169:1364-75.
8. Takahashi T, Suzuki T. Role of sulfatide in normal and pathological cells and tissues. *J Lipid Res.* 2012;53:1437-50.
9. Yalcin EB, Nunez K, Tong M, de la Monte SM. Differential sphingolipid and phospholipid profiles in alcohol and nicotine-derived nitrosamine ketone-associated white matter degeneration. *Alcohol Clin Exp Res.* 2015;39:2324-33.
10. Roux A, Muller L, Jackson SN, et al. Chronic ethanol consumption profoundly alters regional brain ceramide and sphingomyelin content in rodents. *ACS Chem Neurosci.* 2015;6:247-59.
11. Vos JP, Lopes-Cardozo M, Gadella BM. Metabolic and functional aspects of sulfogalactolipids. *Biochim Biophys Acta.* 1994;1211:125-49.
12. Eckhardt M. The role and metabolism of sulfatide in the nervous system. *Mol Neurobiol.* 2008;37:93-103.
13. Kolesnick RN, Krönke M. Regulation of ceramide production and apoptosis. *Annu Rev Physiol.* 1998;60:643-65.
14. de la Monte SM, Kay J, Yalcin EB, Kril JJ, Sheedy D, Sutherland GT. Imaging mass spectrometry of frontal white matter lipid changes in human alcoholics. *Alcohol.* 2018;67:51-63.
15. Petersson KH, Pinar H, Stopa EG, et al. White matter injury after cerebral ischemia in ovine fetuses. *Pediatr Res.* 2002;51:768-76.
16. Gallucci GM, Tong M, Chen X, Stonestreet BS, Lin A, de la Monte SM. Rapid alterations in cerebral white matter lipid profiles after ischemic-reperfusion brain injury in fetal sheep as demonstrated by MALDI-mass spectrometry. *Pediatr Dev Pathol.* 2019;22:344-55.
17. Wang C, Wang M, Han X. Applications of mass spectrometry for cellular lipid analysis. *Mol Biosyst.* 2015;11:698-713.

18. Chen X, Threlkeld SW, Cummings EE, et al. Ischemia-Reperfusion impairs blood-brain barrier function and alters tight junction protein expression in the ovine fetus. *Neuroscience*. 2012;226:89-100.
19. Gunn AJ, Gunn TR, de Haan HH, Williams CE, Gluckman PD. Dramatic neuronal rescue with prolonged selective head cooling after ischemia in fetal lambs. *J Clin Invest*. 1997;99:248-56.
20. Folch J, Lees M, Sloane Stanley GH. A simple method for the isolation and purification of total lipides from animal tissues. *J Biol Chem*. 1957;226:497-509.
21. Jackson SN, Wang H-YJ, Woods AS. In situ structural characterization of glycerophospholipids and sulfatides in brain tissue using MALDI-MS/MS. *J Am Soc Mass Spectrom*. 2007;18:17-26.
22. Yalcin EB, de la Monte SM. Review of matrix-assisted laser desorption ionization-imaging mass spectrometry for lipid biochemical histopathology. *J Histochem Cytochem*. 2015;63:762-71.
23. Bergkvist A, Rusnakova V, Sindelka R, et al. Gene expression profiling – clusters of possibilities. *Methods*. 2010;50:323-35.
24. Eisen MB, Spellman PT, Brown PO, Botstein D. Cluster analysis and display of genome-wide expression patterns. *Proc Natl Acad Sci U S A*. 1998;95:14863-68.
25. Page RD. Visualizing phylogenetic trees using treeview. *Curr Protoc Bioinformatics*. 2002;Chapter 6:Unit 6.2.
26. Kiebish MA, Han X, Cheng H, et al. Lipidomic analysis and electron transport chain activities in C57BL/6J mouse brain mitochondria. *J Neurochem*. 2008;106:299-312.
27. Wang X, Devaiah S, Zhang W, Welti R. Signaling functions of phosphatidic acid. *Prog Lipid Res*. 2006;45:250-78.
28. Jackson SN, Wang H-YJ, Woods AS. Direct profiling of lipid distribution in brain tissue using maldi-tofms. *Anal Chem*. 2005;77:4523-7.
29. Patel D, Witt SN. Ethanolamine and phosphatidylethanolamine: partners in health and disease. *Oxid Med Cell Longev*. 2017;2017:4829180.
30. Morita S-ya, Terada T. Molecular mechanisms for biliary phospholipid and drug efflux mediated by Abcb4 and bile salts. *Biomed Res Int*. 2014;2014:954781.
31. Morita YS, Velasquez R, Taig E, et al. Compartmentalization of lipid biosynthesis in mycobacteria. *J Biol Chem*. 2005;280:21645-52.
32. Nigou J, Gilleron M, Rojas M, García LF, Thurnher M, Puzo G. Mycobacterial lipoarabinomannans: modulators of dendritic cell function and the apoptotic response. *Microbes Infect*. 2002;4:945-53.
33. Podbielska M, Lavery SB, Hogan EL. The structural and functional role of myelin fast-migrating cerebroside: pathological importance in multiple sclerosis. *Clin Lipidol*. 2011;6:159-79.
34. Mencarelli C, Martinez-Martinez P. Ceramide function in the brain: when a slight tilt is enough. *Cell Mol Life Sci*. 2013;70:181-203.
35. Vajn K, Viljetić B, Degmečić IV, Schnaar RL, Heffer M. Differential distribution of major brain gangliosides in the adult mouse central nervous system. *PLoS One*. 2013;8:e75720.
36. Olsen ASB, Færgeman NJ. Sphingolipids: membrane microdomains in brain development, function and neurological diseases. *Open Biol*. 2017;7:170069.
37. Iwabuchi K, Masuda H, Kaga N, et al. Properties and functions of lactosylceramide from mouse neutrophils. *Glycobiology*. 2015;25:655-68.
38. Kiebish MA, Han X, Cheng H, Chuang JH, Seyfried TN. Cardiolipin and electron transport chain abnormalities in mouse brain tumor mitochondria: lipidomic evidence supporting the Warburg theory of cancer. *J Lipid Res*. 2008;49:2545-56.
39. Paradies G, Paradies V, De Benedictis V, Ruggiero FM, Petrosillo G. Functional role of cardiolipin in mitochondrial bioenergetics. *Biochim Biophys Acta*. 2014;1837:408-17.
40. Paradies G, Paradies V, Ruggiero FM, Petrosillo G, stress O. Oxidative stress, cardiolipin and mitochondrial dysfunction in nonalcoholic fatty liver disease. *World J Gastroenterol*. 2014;20:14205-18.
41. Paradies G, Paradies V, Ruggiero FM, Petrosillo G. Cardiolipin and mitochondrial function in health and disease. *Antioxid Redox Signal*. 2014;20:1925-53.
42. Chao H, Lin C, Zuo Q, et al. Cardiolipin-Dependent mitophagy guides outcome after traumatic brain injury. *J Neurosci*. 2019;39:1930-43.
43. Cockcroft S, Carvou N. Biochemical and biological functions of class I phosphatidylinositol transfer proteins. *Biochim Biophys Acta*. 2007;1771:677-91.
44. Drgová A, Likavcanová K, Dobrota D. Changes of phospholipid composition and superoxide dismutase activity during global brain ischemia and reperfusion in rats. *Gen Physiol Biophys*. 2004;23:337-46.
45. Hankin JA, Farias SE, Barkley RM, et al. Maldi mass spectrometric imaging of lipids in rat brain injury models. *J Am Soc Mass Spectrom*. 2011;22:1014-21.
46. Vyas AA, Patel HV, Fromholt SE, et al. Gangliosides are functional nerve cell ligands for myelin-associated glycoprotein (MAG), an inhibitor of nerve regeneration. *Proc Natl Acad Sci U S A*. 2002;99:8412-7.
47. Novgorodov SA, Chudakova DA, Wheeler BW, et al. Developmentally regulated ceramide synthase 6 increases mitochondrial Ca<sup>2+</sup> loading capacity and promotes apoptosis. *J Biol Chem*. 2011;286:4644-58.
48. Sun N, Keep RF, Hua Y, Xi G. Critical role of the sphingolipid pathway in stroke: a review of current utility and potential therapeutic targets. *Transl Stroke Res*. 2016;7:420-38.
49. Kubota M, Narita K, Nakagomi T, et al. Sphingomyelin changes in rat cerebral cortex during focal ischemia. *Neurol Res*. 1996;18:337-41.
50. He X, Schuchman EH. Ceramide and ischemia/reperfusion injury. *J Lipids*. 2018;2018:3646725.
51. Novgorodov SA, Wu BX, Gudz TI, et al. Novel pathway of ceramide production in mitochondria: thioesterase and neutral

- ceramidase produce ceramide from sphingosine and acyl-CoA. *J Biol Chem.* 2011;286:25352-62.
52. Vlassaks E, Gavilanes AWD, Vles JSH, et al. The effects of fetal and perinatal asphyxia on neuronal cytokine levels and ceramide metabolism in adulthood. *J Neuroimmunol.* 2013;255:97-101.
53. Vlassaks E, Mencarelli C, Nikiforou M, et al. Fetal asphyxia induces acute and persisting changes in the ceramide metabolism in rat brain. *J Lipid Res.* 2013;54:1825-33.
54. Novgorodov SA, Gudz TI. Ceramide and mitochondria in ischemia/reperfusion. *J Cardiovasc Pharmacol.* 2009;53:198-208.
55. Novgorodov SA, Gudz TI. Ceramide and mitochondria in ischemic brain injury. *Int J Biochem Mol Biol.* 2011;2:347-61.
56. Novgorodov SA, Riley CL, Keffler JA, et al. Sirt3 deacetylates ceramide synthases: implications for mitochondrial dysfunction and brain injury. *J Biol Chem.* 2016;291:1957-73.
57. Ocaña-Morgner C, Sales S, Rothe M, Shevchenko A, Jessberger R. Tolerogenic versus Immunogenic Lipidomic Profiles of CD11c<sup>+</sup> Immune Cells and Control of Immunogenic Dendritic Cell Ceramide Dynamics. *J Immunol.* 2017;198:4360-72.
58. Kolter T, Proia RL, Sandhoff K. Combinatorial ganglioside biosynthesis. *J Biol Chem.* 2002;277:25859-62.
59. Pyo H, Joe E, Jung S, Lee SH, Jou I. Gangliosides activate cultured rat brain microglia. *J Biol Chem.* 1999;274:34584-89.
60. Jackson SN, Wang H-YJ, Woods AS. In situ structural characterization of phosphatidylcholines in brain tissue using MALDI-MS/MS. *J Am Soc Mass Spectrom.* 2005;16:2052-6.
61. Jeon S-B, Yoon HJ, Park S-H, Kim I-H, Park EJ, Sulfatide PEJ. Sulfatide, a major lipid component of myelin sheath, activates inflammatory responses as an endogenous stimulator in brain-resident immune cells. *J Immunol.* 2008;181:8077-87.
62. McClure MM, Riddle A, Manese M, et al. Cerebral blood flow heterogeneity in preterm sheep: lack of physiologic support for vascular boundary zones in fetal cerebral white matter. *J Cereb Blood Flow Metab.* 2008;28:995-1008.
63. Back SA, Riddle A, Hohimer AR. Role of instrumented fetal sheep preparations in defining the pathogenesis of human periventricular white-matter injury. *J Child Neurol.* 2006;21:582-9.
64. Riddle A, Luo NL, Manese M, et al. Spatial heterogeneity in oligodendrocyte lineage maturation and not cerebral blood flow predicts fetal ovine periventricular white matter injury. *J Neurosci.* 2006;26:3045-55.
65. Perlman JM, Rollins N. Surveillance protocol for the detection of intracranial abnormalities in premature neonates. *Arch Pediatr Adolesc Med.* 2000;154:822-6.